70-25,804

LUNDE, Barbara Kegerreis, 1937-

NUCLEAR MAGNETIC RESONANCE HYPERFINE FIELDS IN THE HEXAGONAL LAVES PHASE COMPOUNDS $ScMn_2$, $ErMn_2$, AND $TmMn_2$.

Iowa State University, Ph.D., 1970
Physics, solid state

NUCLEAR MAGNETIC RESONANCE HYPERFINE FIELDS IN THE HEXAGONAL LAVES PHASE COMPOUNDS $ScMn_2$, $ErMn_2$, AND $TmMn_2$

by

Barbara Kegerreis Lunde

A Dissertation Submitted to the
Graduate Faculty in Partial Fulfillment of
The Requirements for the Degree of
DOCTOR OF PHILOSOPHY

Major Subject: Solid State Physics

Approved:

Signature was redacted for privacy.

In Charge of Major Work

Signature was redacted for privacy.

Head of Major Department

Signature was redacted for privacy.

Dean of Graduate College

Iowa State University
Ames, Iowa

1970

TABLE OF CONTENTS

I. INTRODUCTION

A comparison of the hyperfine fields in a series of very similar intermetallic compounds, some of which contain magnetic ions should shed light on the phenomenon of magnetism. The three compounds studied, $ScMn_2$, $ErMn_2$, and $TmMn_2$, are interesting examples for a nuclear magnetic resonance study. They are hexagonal Laves phase compounds, so there are two inequivalent sites for the Mn. One site is only axially symmetric and the other one does not even have that symmetry. Scandium occupies a site of only axial symmetry, so the spectrum of Sc exhibits coupling between the quadrupole moment of the nucleus and the local electric field gradient. The compounds are available in structurally very well ordered samples, so the nmr lines are very well resolved. In $ScMn_2$, all the shoulders of the satellites are resolved, the first time this has been observed for Sc. In $ScMn_2$ alone, there were 21 lines detectable, with four other lines detectable in the other compounds.

The Sc ion does not have a magnetic moment, whereas the Er and Tm ions do have magnetic moments, so it is possible to compare the hyperfine fields in extremely similar compounds, one without and two with magnetic ions. A study of these should yield some knowledge of how magnetic ions couple with the rest of the crystal and therefore each other in the magnetically disordered state.

II. THEORY

A. Capabilities of Nuclear Magnetic Resonance

Using the technique of nuclear magnetic resonance, one can measure certain parameters of the environment of a nucleus in a material. One can, in a sense, probe into a material and measure the precise electric and magnetic fields exactly at the position of the nucleus of a certain ion. The parameters that are usually measured in a solid are the three components of the Knight or chemical shift, as it is called in physics and chemistry, respectively, the two independent components of the quadrupole coupling, and the width of the resonance line. These may be measured at various temperatures. Symmetries in the crystal structure may reduce the number of measurable parameters.

B. The Isotropic Knight Shift

The Knight shift (1) is the shift of the frequency of the resonance, for a particular value of the applied magnetic field, in the material which is being measured compared to the frequency of the resonance for the same nucleus in a reference solution. It is a measure of the additional magnetic field at the nucleus contributed by the electrons of the material. It can have three different components if the material is completely asymmetric. The isotropic shift, K_{iso}, is the average of the components.

There are three recognized contributions to the Knight shift in transition metals (2), K_s, K_d, and K_{vv}.

K_s, the s contact part, is the first contribution to the Knight shift to be recognized. It explains the measured shift in the alkali and noble metals. An expression for this contribution is (3)

$$K_s = \frac{8\pi}{3} V \chi_p^s \langle |\psi(0)|^2 \rangle \qquad (1)$$

where V is the atomic volume, χ_p^s is the Pauli magnetic susceptibility of the electrons with s like wave functions, $\langle |\psi(0)|^2 \rangle$ is the density of the wave function for the s like wave function averaged over the Fermi surface.

The second contribution to the Knight shift is K_d, the core polarization contribution, due to polarized d electrons. An expression analogous to (1) for K_d is

$$K_d = - \frac{8\pi}{3} V \chi_p^d \langle |\Phi_{cp}(0)|^2 \rangle \qquad (2)$$

where χ_p^d is the Pauli susceptibility of the d like electrons and $\langle |\Phi_{cp}(0)|^2 \rangle$ is the product of the density of the wave functions for the normal s like electrons with the density of those perturbed into a higher s state by the presence of polarized d like electrons averaged over the Fermi surface. An analytical expression for it is

$$|\Phi_{cp}(0)|^2 = - \sum_n \frac{2J_n}{\langle E_n \rangle - \langle E_1 \rangle} a_{1s}(0)\, a_{ns}(0) \qquad (3)$$

where J_n is the Coulomb integral between states $\psi_{3d,\ 1s}$ and $\psi_{3d,\ ns}$, for the transition metals, that are mixed via configuration interaction, $\langle E_1 \rangle$ and $\langle E_n \rangle$ are their mean energies, and $a_{1s}(0)$ and $a_{ns}(0)$ are the amplitudes of the s functions at the origin.

The third contribution to the Knight shift is K_{vv}. This is the orbital contribution to the Knight shift. It is called K_{vv} because it is proportional to the contribution to the magnetic susceptibility explained by Van Vleck.

$$K_{vv} = 2V\, \chi_{vv} \left\langle \left| \frac{1}{r^3} \right| \right\rangle_{met} . \tag{4}$$

where χ_{vv} is the Van Vleck susceptibility, calculated by the quantum mechanical perturbation theory.

$$\chi_{vv} = 2N \sum_{n} \frac{|(n|\, \mu_z |0)|^2}{E_n - E_o} \tag{5}$$

where N is the number of atoms per unit volume, n is a possible excited state above the ground state, 0 is the ground state, μ_z is the magnetic moment operator, and $E_n - E_o$ is the difference in energy between the ground and excited states (4). $\left\langle \left| \frac{1}{r^3} \right| \right\rangle_{met}$ is the average of the inverse cube of the distance of the electrons from the nucleus in the various states. This is assumed to be the same for all the states.

These contributions to the Knight shift may be combined in one expression which may be used to define the hyperfine fields as[1] (2,5)

$$K = K_s + K_d + K_{vv}$$

$$= [H_{hfs}^{(s)} \chi_s + H_{hfs}^{(d)} \chi_d + H_{hfs}^{(orb)} \chi_{vv}] \cdot \frac{g\beta}{N} \tag{6}$$

where $H_{hfs}^{(s)}$, and $H_{hfs}^{(d)}$ are the effective s-contact and d-spin (core polarization) hyperfine fields per electron, respectively, and $H_{hfs}^{(orb)}$ is the orbital hyperfine field per unit orbital angular momentum. In certain cases the actual hyperfine field contribution may be determined for the various components.

---

[1] Narath in ref. 5 has an extra factor of (- 1/2), which may be due to his definition of γe, which is used in his equation. The factor of -1/2 is not included here.

The preceding is a description of the contributions to the Knight shift in a transition metal. The first term in (6) describes the Knight shift in the alkali and noble metals. For compounds with the rare earths, the series of metals with unfilled f shells, another term, taking into account the localized moment of the unfilled f shells, must be included. There have been various theories for calculating this, for example, the uniform conduction-electron polarization model (6,7) and the Ruderman-Kittel-Kasuya-Yosida (RKKY) (8,9) models.

This contribution to the Knight shift arises from an interaction of the form $K_f(T) = A\vec{I} \cdot \langle \vec{S} \rangle$, where A is a hyperfine interaction constant, $\vec{I}$ is the nuclear spin and $\langle \vec{S} \rangle$ is the time averaged value of the rare-earth 4f spin component of the angular momentum $\langle \vec{J} \rangle$ (10).

Putting this in the same form as Eq. (6) it will be

$$K_f(T) = (g_J - 1)\, H_{hfs}^{(f)}\, \chi_f(T)/N g_J \beta \,. \qquad (7)$$

where g_J is the Lande g factor for the rare earth ion (3), N is Avagadro's number, and β is the Bohr magneton.

In the uniform conduction-electron polarization model for rare earth intermetallic compounds, the conduction-electron spins are uniformly polarized by an s-f exchange interaction of the form $-\Gamma S \cdot \sigma$ with the rare earth spin $\vec{S}$. The resulting Knight shift $K_f(T)$ is given by

$$K_f(T) = - K_o\, \Gamma \langle S(T) \rangle / 2 \beta H \qquad (8)$$

where K_o is the temperature independent part of the Knight shift.
The total Knight shift is expressed as $K(T) = K_o + K_f(T)$, (9)
separating the constant from the temperature dependent part.

The Knight shift, according to the RKKY theory, can be written in

the same form if one allows Γ to equal a combination of factors, i.e. (10).

$$\Gamma = -12\ \pi\ Z\ \Gamma\ (0) \sum_{R} F(2k_F R) \qquad (10)$$

where Z is the number of conduction electrons per atom, k_F is the Fermi wave vector, $\Gamma(0)$ is the $k = 0$ value of the s-f exchange constant Γ and

$$F(x) = (x \cos x - \sin x)/x^4 \quad .$$

Since the quantity that can be measured, in this case, is the proportionality constant between the Knight shift and the susceptibility, one parameter, and k_F is not known, the analysis will be in terms of Γ, one parameter, and not a combination of two parameters such as Eq. 10. If k_F becomes known, or other theories are advanced, they can be related to the value of Γ given here.

C. Anisotropic Knight Shift

The nucleus of an atom which occupies a position of less than cubic symmetry may have a non-isotropic Knight shift. If the Knight shift were measured in a single crystal of the material, its value would depend on the orientation of the crystal axes to the applied magnetic field (11). Non s state electrons which have a greater electron population along certain crystal axes than others will lead to an anisotropic Knight shift.

The Knight shift parameters are defined by

$$3\ K_{iso} = K_x + K_y + K_z,$$

$$6\ K_{ax} = 2\ K_z - K_x - K_y \text{ and}$$

$$2\ K_{aniso} = K_x - K_y,$$

where K_x, K_y, and K_z are the Knight shift components in the principal axis system. The definition of K_{ax} is the one that has been used in earlier work in this group (12).

Some other authors use the definition

$$3\ K_{ax} = 2\ K_z - K_x - K_y . \quad (11, 13)$$

D. Electric Field Gradient Measurement

The electric field gradient at the nucleus can be measured using the techniques of nmr. The nmr spectrum is affected by the change in the magnetic energy levels due to the interaction between the quadrupole moment of the nucleus and the electric field gradient at the nucleus. Of course, if either of these are null, there will be no effect.

The theory for a powdered sample which has a spectrum affected only by an axially symmetrical electric field gradient has been stated by Jones, Graham, and Barnes (14).

The spectrum which would have had only a single line without the effect of the electric field gradient is split into several lines. For a nucleus with spin value $I=(n + 1/2)$ where n is an integer, there is a central line with n satellites on either side of it. The distance between the first satellites on either side of the central line is ν_Q, the quadrupole frequency. This is the frequency of a resonance which would be observed at zero applied magnetic field, due to the interaction of the quadrupole moment with the electric field gradient,

$$\nu_Q = 3e^2qQ/\ 2I(2I-1)h,$$

where e is the charge of the electron, q is the electric field gradient at the nucleus, Q is the quadrupole moment of the nucleus and h is Planck's

constant.

In the case of axial symmetry, $V_{zz} = -V_{xx} - V_{yy}$ and $V_{xx} = V_{yy}$, where V_{zz}, V_{xx}, and V_{yy}, denote the second derivatives of the potential with respect to the coordinates of the principal axes. In the literature, $V_{zz} = eq$. For the case of non-axial symmetry, $\eta \equiv (V_{xx} - V_{yy})/V_{zz}$ with η restricted so that $0 \leq \eta \leq 1$.

E. Electric Field Gradient Calculation

The electric field gradient at the nucleus of a solid may be calculated. The causes of the electric field gradient at the nucleus of a solid are the gradient due to the ions surrounding the nucleus and the gradient due to any incomplete electron shells in the ion in question. These fields are modified by shielding due to the closed shell electrons of the ions in question and the conduction electrons.

The electric field gradient at the nucleus due to the other ions in the lattice is, in principle, easy to calculate. For instance,

$$V'_{zz} = \sum_{i'} q_i(r) \frac{(3z^2 - r^2)}{r^5},$$

where the sum is over all the charges q_i in the crystal except the one at the origin. The charges are at distance r from the origin and distance z in the z direction from the origin. The problem is that many atoms must be summed. DeWette (15) developed a way of doing this fairly easily. A computer program using the DeWette method was written in Fortran to calculate the field gradient due to the ions. This will be found in Appendix A. This calculated electric field gradient at the nucleus is modified by the shielding of the closed electron shells of the ion. This shielding, or antishielding, has been calculated by Sternheimer (16)

for certain ionic states of certain elements. It can be expressed as $V_{zz} = V'_{zz}(1 - \gamma_\infty)$, where V_{zz} is the actual field gradient at the nucleus, including the shielding, V'_{zz} is that calculated from the ion positions, and γ_∞ is the Sternheimer shielding factor. The value of -7 for γ_∞ for the Sc^{3+} state (17) will be used. The value of -11.27 will be used for the Mn^{2+} state (16).

The conduction electrons will also provide shielding of the crystal electric field calculated from the external ion positions. This has not been calculated theoretically, although this shielding has been the subject of considerable speculation, and it has been calculated by noting the difference between measured values and calculated values of the electric field gradient omitting this effect (18, 19). There is some hope that it will soon be calculated for some cases (19), from first principles.

For the case of Sc, there are no incomplete inner shells, so that source of an electric field gradient is not applicable. In the case of Mn, the d shell is probably incomplete. The exact electronic configuration will not be known until detailed band structure calculations have been made for the compound.

The measured electric field gradients at the nuclei of Sc in $ScMn_2$ and Mn at its two lattice sites in $ScMn_2$, $ErMn_2$, and $TmMn_2$ are reported in this thesis, as well as the DeWette sum calculations for these cases.

F. Combined Effects of Knight Shift and Electric Field Gradient with Complete Asymmetry on the Central Line

Jones, Graham, and Barnes work out the expected spectrum for the case of the combined effects of axially symmetric nuclear quadrupole and anisotropic shift interactions (14).

In the compounds studied here, one of the Mn sites does not have axial symmetry, so it was necessary to work out the expected powder pattern spectra for a combination of non-axially symmetric Knight shift and non-axially symmetric nuclear qudrupole interactions to understand our spectra.

The algebraic equations for the positions of the resonance in a single crystal sample, at various orientations with the applied magnetic field were calculated (20). The critical points in a powder pattern were determined, following Narita et al. (21) who calculated the critical points ignoring the effects of anisotropic Knight shifts. The points we calculated agreed with the later published work of Baugher, et al. (22).

If the broadening of the line due to effects other than the electric field gradient and the Knight shift, i.e. dipolar broadening, called the breadth of the line here, is small compared to the total width of the line, the position of a feature on the spectrum corresponds to its theoretical position with no broadening and the hyperfine fields may be computed accurately by graphical techniques. As can be seen from the expressions for the frequency dependence of the locations of shoulders and singularities in Table I of Baugher's work (22) which is reproduced in Appendix B, if $\Delta H\nu$ is plotted versus ν^2, for $\nu_5 - \nu_6$, $\nu_6 - \nu_4$, $\nu_1 - \nu_3$, $\nu_3 - \nu_5$, or some other combinations of singularity points, the data points should lie along lines, and the intercepts of the lines with the axes equal algebraic combinations of R and η. R is used by Baugher to equal $\nu_Q^2[I(I + 1) - 3/4]$. The slopes of the lines are algebraic combinations of the σ's and η, if the terms of order ν^3 in the equations of Table I are negligible, as they are in this case. If they are not negligible, an iterative procedure may

be used to calculate the parameters. The σ's are used to designate the chemical shift. This is the same phenomenon as the Knight shift in metals, except for sign. $3\ K_{iso} = -(\sigma_1 + \sigma_2 + \sigma_3)$, $6\ Kax = -2\ \sigma_3 + \sigma_1 + \sigma_2$, $2\ K_{aniso} = \sigma_3 - \sigma_2$. It was found that the most accurate way to calculate R and η was to graph each algebraic function and choose the points for R and η which were nearest their intersection. This can be done mathematically by choosing an R and taking an average of the points for η from each curve, weighted according to the number of points constituting each curve. Another value is then picked for R and the procedure repeated. The final value for R that is chosen is the one with the least calculated probable error in η. The probable error for R is then calculated from the values of R for that η for each equation.

From Baugher's paper, ν_1 is the highest frequency shoulder of the pattern. It corresponds to Narita's y_{11}. Some of Narita's equations are also reproduced in Appendix B for reference.

Narita apparently lost a minus sign between his eq. 5 and eq. 7, so when he indicates negative shifts in frequency, they should be positive. ν_1 will be at the lowest field in a constant frequency plot. ν_2 corresponds to Narita's y_{12}, ν_3 to y_{13}, ν_4 to y_s, ν_5 to y_{21}, and ν_6 to y_{22}.

As Narita *et al.* show in their Figure 4 (21), the positions of the peaks and crossings in the derivative spectra are very dependent on the breadth of the lines. However, for breadths less than 0.0287 of the total spread of the spectrum, the positions of the extrema in the integrated spectrum are independent of the breadth as asserted before. This was the case for the spectra investigated here. The breadth of the line is here

equated to the square root of one half the denominator of the exponent of a Gaussian curve describing broadening of the line. The breadth is σ and the Gaussian curve describing the line is $g(y - y') = \frac{1}{\sqrt{2\pi}} e [-(y - y')^2/2\sigma^2]$.

G. The Effects of an Asymmetric Knight Shift and Electric Field Gradient on the Satellites

As was pointed out in the section on electric field gradient measurement, the nmr line that, with no hyperfine interactions would be a single, sharp line, is split into several lines. For nuclei with spin values, $I = (n + 1/2)$, where n is an integer, there are n so-called satellites on either side of the central line. As is remarked by Jones, Grahm, and Barnes (14), the distance between corresponding opposite satellites always has a constant value proportional to the quadrupole frequency to third order, but the center of the satellite pattern is off-set from the position of the central line by a second order quadrupole effect.

$$\nu(m \rightarrow m - 1) = \nu_o - (1/4)\nu_Q(2m - 1) - (\nu_Q^2/16\ \nu_o)[3m(m-1) - I(I+1) + 3/2]$$

where $m = \bar{I}, \bar{I} - i, \ldots, -\bar{I}$.

If, in addition to the quadrupole interaction, there is an anisotropic, but axially symmetric Knight shift, all the satellites will be displaced by an amount $-K_{ax}\nu_o$, for the main satellites and $+2K_{ax}\nu_o$ for the shoulders.

If the symmetry is not axially symmetric, the satellite structure will be affected. If the electric field gradient effects are considered alone, shoulders are found at $(\nu_Q/2)(1 + \eta)(m - 1/2)$ and $-\nu_Q(m - 1/2)$. A singularity is found at $(\nu_Q/2)(1 - \eta)(m - 1/2)$. In other words, the strong satellite is broken up into two lines. The outer is now a shoulder and is $(1 + \eta)$ farther out, and the inner is still a singularity and is $(1 - \eta)$ further in. The weaker, shoulder satellite remains in the same

position.

The three lines are each affected by the Knight shift associated with a different principle axis. The shoulder at $(1 - \eta)$ has the additional shift $(1 + K_x)$ or $(1 + K_{iso} - K_{ax} + K_{aniso})$. The singularity at $(1 - \eta)$ is shifted by $(1 + K_y)$ or $(1 + K_{iso} - K_{ax} - K_{aniso})$. The other shoulder, unaffected by η, is shifted by $(1 + K_z)$ or $(1 + K_{iso} + 2K_{ax})$.

H. Dipolar Broadening

One of the chief contributions to the width of an nmr line, other than the anisotropic Knight shift and quadrupole splitting, is dipolar broadening (11). The "dipole" in the name is the dipole magnetic moment of the nuclei surrounding the nucleus of interest. The neighboring nuclei will produce fields on the order of a few Oe at a nucleus (11). There are different contributions from identical and different nuclei. Identical nuclei will have static fields at the neighboring sites, as well as rotating fields due to their rotation (in the classical sense) which will be in resonance with neighboring identical nuclei. Different nuclei will only have the effect of the static field, because their rotating fields will not be in resonance with their non-identical neighbors.

The equation for the second moment of the line shape in a compound of two types of nuclei is

$$\Delta H_2^2 = 3/5\ I(I + 1)\gamma^2 h^2 \sum_j r_j^{-6} + 4/15\ I'(I' + 1)\gamma_f^2 h^2 \sum_i r_f^{-6}.$$

Experimentally, for the line illustrated in figure 1b, the second moment is half the distance between the extrema of the derivative line shape, figure 1c, squared. The nuclear spin of the nucleus of interest is I, and the spin of the other species of nuclei is I'. γ is the gyromagnetic ratio of the

nucleus in question. γ_f is the gyromagnetic ratio of the other nucleus. h, of course, is Planck's constant. r_j and r_f are the distances from the nuclei in question to its identical neighbors and to its other neighbors, respectively.

If the spectral line in question is not a simple gaussian in which, without the dipolar broadening, the interaction would only occur at one frequency, the line shape will be affected by the shape of the resonance as it is broadened by anisotropic Knight shift or quadrupole interactions. The actual line shape will be

$$G(H) = \int_{-\infty}^{+\infty} P(H') \, g(H - H') \, dH'$$

where G(H) equals the actual distribution function of the interactions for a constant frequency in a varying magnetic field, H. This is the so-called line shape. P is the distribution function of the interaction except for the dipolar broadening, and g is the gaussian distribution due to dipolar broadening.

If the extent of P(H') is much larger than g(H - H'), the actual shape and the amount of dipolar broadening may be evaluated fairly accurately, without too much work. For instance, if the spectrum is the derivative of a flat shoulder, or step function broadened by dipolar broadening, illustrated in Figure 1f, it will be a gaussian. This is the simplest shape found in the central transition of the spectrum of the Mn nucleus without axial symmetry. The usual simple spectrum, of course, is assumed to be a broadened spike or delta function, which is illustrated in Figure 1b. Its derivative spectrum is the derivative of a gaussian. This is illustrated in Figure 1c. A mathematical analysis, including numerical

Figure 1. Functions used for line shape calculations

a. Spike

$\delta(H) = 0,\ H \neq 0;\ \delta(H) = \infty,\ H = 0$

b. Broadened spike

$g(H) = (1/\sqrt{2\pi})\ e^{-H^2/2}$

c. Derivative of a broadened spike

$g'(H) = -(H/\sqrt{2\pi})e^{-H^2/2}$

d. Step function with no broadening

$F(H) = 0,\ H < 0;\ F(H) = 1,\ H > 0$

e. Broadened step function

$f(H) = \int_0^\infty g(H - H')dH'$

f. Derivative of a broadened step function

$g(H) = (1/\sqrt{2\pi})\ e^{-H^2/2}$

g. Step function with slope 1/10

$S(H) = F(H)(1 + H/10)$

h. Broadened step function with slope 1/10

$s(H) = (1 + H/10)f(H) + (1/10)g(H)$

i. Derivative of a broadened step function with slope 1/10.

$s'(H) = (1/10)f(H) + g(H)$

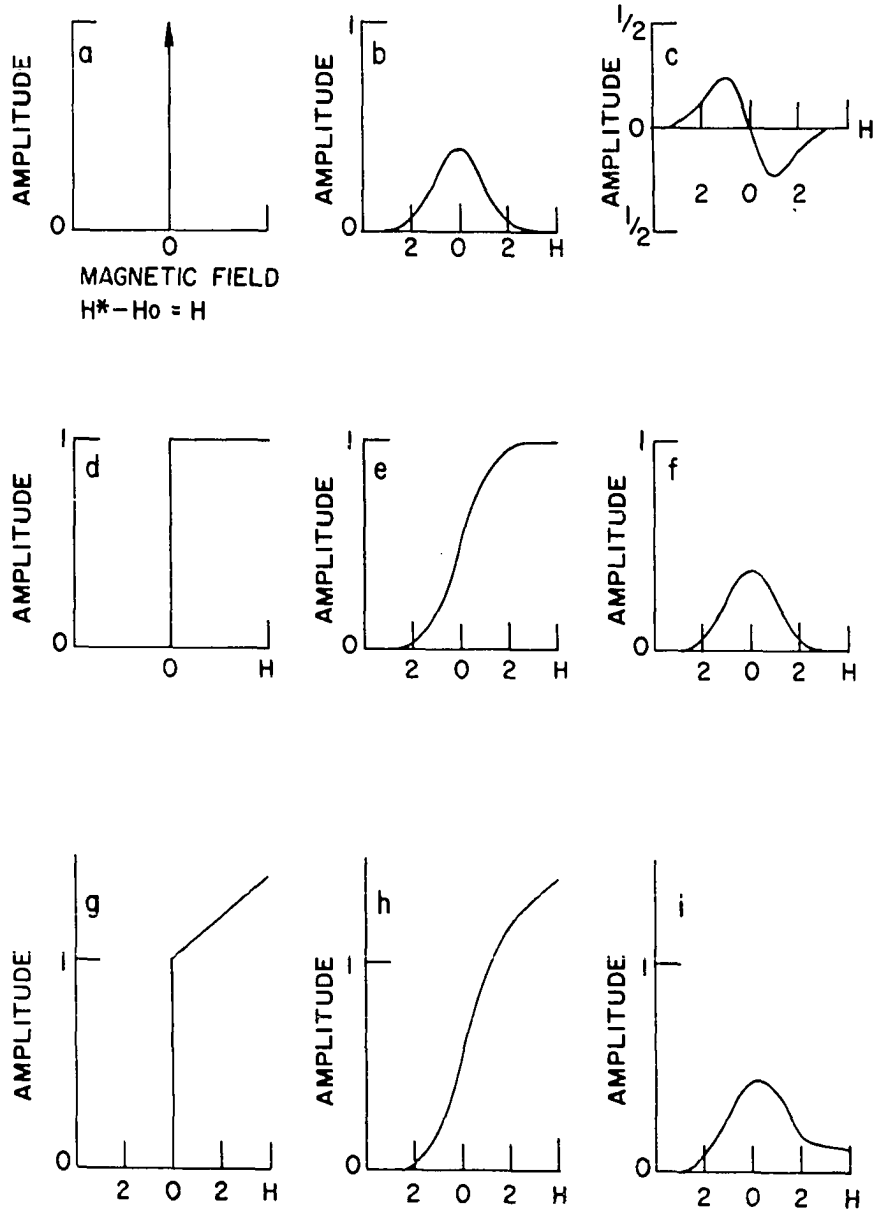
a
AMPLITUDE
1
0
0
MAGNETIC FIELD
H*−Ho = H
b
AMPLITUDE
1
0
2 0 2 H
c
AMPLITUDE
1/2
0
1/2
2 0 2 H
d
AMPLITUDE
1
0
0 H
e
AMPLITUDE
1
0
2 0 2 H
f
AMPLITUDE
1
0
2 0 2 H
g
AMPLITUDE
1
0
2 0 2 H
h
AMPLITUDE
1
0
2 0 2 H
i
AMPLITUDE
1
0
2 0 2 H

integration was done to compare the width of these two types of lines. The full width at half maximum of the derivative spectrum of a broadened step function is 1.17 times the distance between the extrema of the derivative of a similarily broadened spike. Of course, the maximum derivative of the broadened step function is at the position of the step, so the measured position of the flat shoulder is unaffected by the broadening.

If the original function of not a step, but rather the product of a step and a line with a slope of 0.1 A/t where A is the amplitude of the step and t is a parameter of the Gaussian broadening function

$$g(t) = 1/\sqrt{2\pi}\ e^{-t^2/2},$$

as illustrated in Figure 1h, then the full width at half maximum is 1.3 times the distance between the extrema of the derivative of a similarily broadened spike. The maximum derivative is moved toward the non-zero side of the step by 0.1 t.

III. EXPERIMENTAL METHODS

A. Sample Preparation

The samples used in this study were prepared at the Ames Laboratory of the A.E.C. using the best materials and methods available. An early set of samples of $ErMn_2$ and $TmMn_2$ were prepared by arc melting. They were examined metallographically and then annealed for three weeks at 920°C. The heat treated samples were again examined metallographically. The crystal grains were larger after annealing. Another set of samples of $ErMn_2$ and $TmMn_2$ were made from rare earths of the purities shown in Table I. The Mn was electrolytic Mn from the Foote Mineral Co. The samples were arc melted and were turned, while red hot, four to five times and melted again. They were turned while red hot because they would shatter when melted again if they were allowed to cool before remelting. They were then annealed for two weeks at 900°C. The second $TmMn_2$ sample and the first one had identical nmr spectra. The first sample had been stored under helium for about a year. The second sample was freshly prepared and stored under helium. The second set of samples was made because it was thought that the first set had deteriorated with time.

The $ScMn_2$ sample was handled in air. It did not seem to deteriorate with time. The $ErMn_2$ and $TmMn_2$ samples were crushed with a ceramic mortar and pestle and sieved through a 325 mesh sieve in an argon atmosphere and stored and observed in pyrex tubes with a helium atmosphere.

There was no indication of impurity or distortion in the crystal structure in any of the nmr spectra, aside from the usual broadening of the lines, which was less than accustomed. The $ScMn_2$ spectra had probably the best definition of any spectrum of its type viewed in this laboratory.

Table 1. Impurities in Er and Tm metals which were used in samples of $ErMn_2$ and $TmMn_2$

Er- Sample number JC-3-105		Tm-Sample number RE-17A	
H	8	H	7
N	4	N	7
O	35	O	N.D.
F	13	Mg	$^{d}<10$
Mg	$^{-}<20$ [1]	Al	$^{d}<20$
Al	$^{-}<40$	Si	$^{-}<30$
Si	$^{-}<30$	Ca	$^{d}<10$
Ca	$^{d}<20$ [2]	Cr	$^{d}<20$
Cr	$^{-}<20$	Fe	$^{-}<40$
Fe	$^{-}<20$	W	$^{-}<50$
Ta	$^{-}<300$	Y	$^{-}<10$
W	30	Ho	$^{x}<200$ [3]
Y	$^{d}<50$	Er	$^{d}<30$
Dy	$^{-}<100$	Yb	$^{d}<30$
Ho	$^{d}<100$	Lu	$^{Y}<200$
Tm	$^{d}<100$		
Yb	<50		

[1] - = not detected.

[2] d = detected.

[3] x = interference.

B. The Equipment

The nmr measurements were made using the standard nuclear induction technique described by Bloch (23), using a crossed coil induction spectrometer.

For the frequency range 2 to 26 MHz, a wide line nmr induction spectrometer designed by D. R. Torgeson (24) was used with a Varian Associates 15 inch electromagnet system that could supply a field of 25.3 KOe homogeneous to 0.5 Oe over a 1.5 cm^3 volume with a gap of 1 3/4 inches. The magnet had a Fieldial magnetic field regulator, Mark II.

A Varian Associates Model V4210A variable frequency wideline spectrometer was also used in the frequency range from 2 MHz to 16 MHz with a Varian Associates Model V4012 12 inch electromagnet. This equipment was used alternatively with the first system for the lower field measurements.

The spectrometers were used at constant frequency. High frequency stability was obtained by using crystal synchronization. By this method, frequency changes of less than 10 Hz over days were attained. Frequency measurements were made using Computer Measurements Corporation frequency counters Model 880B and Model 707BN with a Model 731B frequency converter.

The continuous averaging method (25) was used to improve the signal to noise of some of the spectra. RIDL Model 24-2 400 channel analyzers were used to store the data.

Glass dewars were used for the low temperature work. Single finger dewars with clear glass tails, not silvered, were used at liquid nitrogen temperature. Dewars with three inch diameter and 22 inch length reservoirs would hold nitrogen more than 12 hours. A double dewar from H.S. Martin and Son was used for liquid helium temperature. Only the helium bath

extended into the dewar tail. There was a thin plating of platinum which was scratched to allow penetration of the radio frequency energy. The dewar was completely sealed. Another double, liquid helium dewar was also used. It was made in the glass shop at Iowa State University. The vacuum spaces were interconnected and there was a connection for pumping them so that the helium which diffused through the glass could be pumped out between uses to maintain the vacuum. It had a scratched, silvered tail. Both dewars held helium approximately ninety minutes.

C. Procedure for Taking Data and Calibrating

All of the data were taken as nearly as possible in the absorption mode. Because the resonances are split so widely into so many lines, rather wide scans with rather large modulation amplitudes were used in many cases. In spectroscopy, one always faces the trade-off between a trace with accurate line position and shape, but a lot of noise, and a trace with a good signal-to-noise ratio, but distortion because of the large modulation amplitude, slit width, or whatever. Even with continuous averaging or narrow bandwidth lock-in amplifiers, there is a reasonable maximum time for a trace, such as 24 hours, which limits the possible signal-to-noise. This limit is imposed by possible drift of the equipment, use of coolant in batch load dewars, and human impatience. In the case of spectra of large extent, there is also a trade-off between many spectra of short extent to encompass the phenomenon, which will be hard to interpret as a whole, but will be individually accurate, and a spectrum of long extent which may be distorted by the measures taken to get effectively a large bandwidth of information, i.e. fast scan, and large modulation amplitude.

In this work scans as large as 10,000 Oe and as small as 21 Oe were used.

Often in nmr studies, as for much of this work, the important aspect is the magnetic field position of the lines. To determine this, the most accurate method is to calibrate with an nmr reference with a gyromagnetic ratio which has previously been determined. Aluminum, in a water solution of $AlCl_3$, was used in this work, with the gyromagnetic ratio of 11.094 MHz/10KOe.

The static calibration method, which is the standard method, is described by Lecander (26). In this method, errors may be caused by the magnetic field being somewhat delayed in reaching its desired value, so that the actual dynamic scan, during which data is taken, is slightly off-set from the calibration attained in a static situation. Another error may be caused by a distortion in the recorded resonance due to the time constant setting of the lock-in amplifier and other effects. The resonance is generally delayed and spread out by a long time constant.

For accurate work, with this type of calibration, these errors are minimized by scanning both ways, both up-field and down-field. The measured values for the two traces are then averaged. This doubles the experiment time, and, since there may be a rather large error in both traces, the average may be in error by, say, one tenth the error in each trace. These errors are also minimized by scanning as slowly as possible and using a small modulation and time constant. However, one pays by increased noise for these measures.

Another method of calibration was used in this work, a dynamic method. Instead of pausing at chosen channel numbers or field values, the reference

was inserted into the spectrometer and the frequency was set so that the resonance would occur in the scanned field. The spectrum was then recorded with exactly the same choices of time constant, etc. as used for the regular scan. In some cases the rf power to the spectrometer was reduced to make the trace of manageable amplitude, since the resonance in the reference was stronger than that in the compounds under study. The resonance of the reference was then recorded on the same graph as the experimental trace with its frequency. The reference was also recorded one or more times in other positions on the graph by using slightly difference frequencies. The calibration was then made by a direct measurement on the graph. An additional dividend of the dynamic method is that one has a graphic display of the effect of the experimental spectroscopic parameters used, such as the modulation amplitude. No features in the experimental trace substantially smaller than the demonstrated width of the reference resonance are real features of the trace, but are probably noise. Of course, an experimental resonance of other than narrow Gaussian shape like the reference may have its features somewhat displaced from the fields measured in this way, so it is still wise to use the methods for making the static calibration accurate, i.e. slow scan, small modulation, and short time constant, for maximum accuracy.

The spectra had so many lines, and the lines had such unusual shapes that, for the preliminary analysis, as many as 31 or more line positions needed to be calculated for one trace. It was extremely tedious to do this by hand calculator and mistakes would creep in which would ruin the attempted analysis. Many different parameters for each line had to be calculated in order to do the analysis. A computer program was written which calculated

the square of the experimental frequency, the inverse square of the experimental frequency, the scale of the magnetic field axis on the trace,or number of Oersteds per line of chart paper on the original data, and, for each line, the effective gyromagnetic ratio, gamma, the effective Knight shift, the magnetic field at which the line occurred, and the inverse square of the magnetic field. This information is printed on paper and also punched on cards for further processing of the information. The inputs to the program are the experimental frequency, the position on the graph of two calibration resonances, the frequencies of the calibration resonances, and the positions of the unknown lines. The program will be found in Appendix C.

D. Magnetic Susceptibility Measurements

Susceptibility measurements were made in the Metallurgy Division of the Ames Lab on samples of the compounds studied. The rare earth compounds were measured at a series of temperatures between room temperature and 77^{o} K. The methods and equipment used were the same as discussed by other members of this group (26, 27) with the addition of the variable temperature equipment. The method used was the Faraday method, described by Selwood (28).

IV. RESULTS AND DISCUSSION

A. NMR Results

1. $\underline{ScMn_2}$

The room temperature parameters of the $ScMn_2$ spectrum have already been published by this group (12). They are repeated here in Table 2. Mn_I is the Mn in the axially symmetric site. Mn_{II} is the Mn in the other site. Figure 2 is the absorption derivative trace of the nmr of $^{45}Sc^{55}Mn_2$ at room temperature. The methods of deriving these parameters from the data have already been discussed in the section on theory. The $\delta\nu$ expt. are calculated from the width between extrema of the central line of the Sc spectrum, which seems to be constant from 7 to 25.4 MHz, the width between the extrema of one side of the widely split central transition in the spectrum of the Mn_I such as $Mn_I(H)$ in Figure 2 and the full width at half maximum of the line from a shoulder in the Mn_{II} spectrum such as $Mn_{II}(y_{II})$ in Figure 2, or y_{II} in Figure 3, Appendix B. The values of $\delta\nu$ theor. (Oe) have been modified in the table because of more complete recent calculations of the contributions from the various atomic sites in the crystal, rather than a partial calculation and an extrapolation from the results for other crystals, which had been used for the published numbers. The revised numbers are about 10% different from the published ones.

The quadrupole frequency of Sc was measured using both the peaks of the satellite spectrum and the shoulders. The position of the peaks is measured as described by Adams (29). The position of the line is taken to be closer to the center of the pattern than the maximum in the derivative absorption spectrum by 0.241 of the distance between the extrema in the derivative shape for that particular satellite, such as Sc(-3) in Figure 2.

Table 2. Summary of Knight shift and quadrupole coupling parameters for the ^{45}Sc and ^{55}Mn resonance spectra in $ScMn_2$ (at 300°K)

	^{45}Sc	$^{55}Mn_I$	$^{55}Mn_{II}$
Site Symmetry	3m	$\bar{3}$m	mm
K_{iso} (%)	-0.091 ±0.006	+0.9 ± 0.2	+0.69 ± 0.05
K_{ax} (%)	< 0.01	+0.12 ± 0.16	-0.03 ± 0.01
K_{aniso} (%)	0	0	-0.025 ± 0.005
ν_Q (MHz)	0.0555 ± 0.0003	3.2 ± 0.2	1.57 ± 0.015
e^2qQh^{-1}	0.777 ±0.004	21.3 ± 1.3	10.58 ± 0.09
η	0	0	0.71 ± 0.02
$\delta\nu$ expt. (Oe)	6.9 ± 0.3	7.6 ± 0.6	10.4 ± 0.6
$\delta\nu$ theor. (Oe)	4.70	6.45	6.27

Fig. 2. Absorption derivative trace of the nmr spectrum of $^{45}Sc^{55}Mn_2$ at 22.003 MHz. The upper trace shows primarily the ^{45}Sc spectrum. The central transition, the three satellites, and the two steps of the spectrum are noted. The lower trace consists of most of the central transition features of the ^{55}Mn spectra, with the high-field portion of the central transition of the ^{55}Mn in the symmetric site appearing on the right side of the upper trace. Notation of the features of the asymmetric spectrum follows that of Narita, et al. (21). This is Figure 1 of Barnes and Lunde (12).

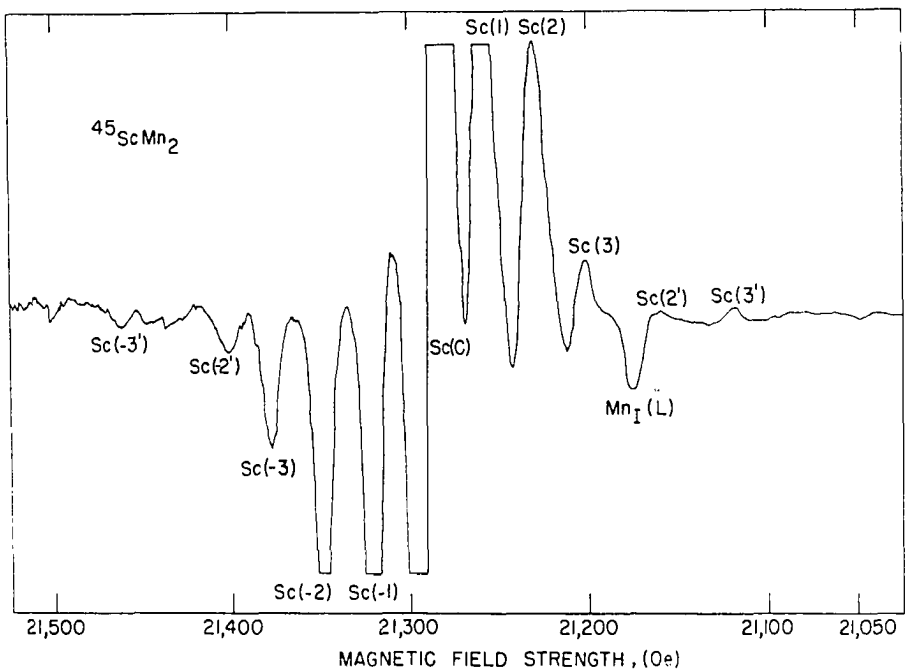
Sc(1) Sc(2)
$^{45}ScMn_2$
Sc(3)
Sc(2') Sc(3')
Sc(-3')
Sc(2')
Sc(C)
Mn_I (L)
Sc(-3)
Sc(-2) Sc(-1)
21,500
21,400
21,300
21,200
21,100
21,050
MAGNETIC FIELD STRENGTH, (Oe)

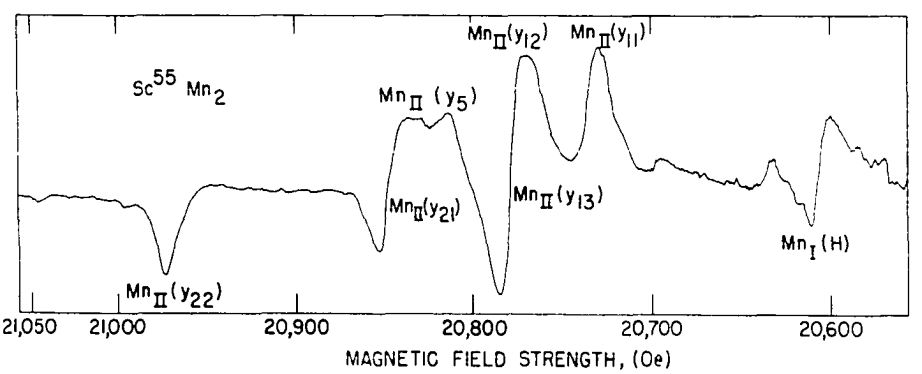
$Mn_{II}(y_{12})$ $Mn_{II}(y_{11})$
$Sc^{55}Mn_2$
Mn_{II} (y_5)
$Mn_{II}(y_{21})$
$Mn_{II}(y_{13})$
Mn_I (H)
$Mn_{II}(y_{22})$
21,050
21,000
20,900
20,800
20,700
20,600
MAGNETIC FIELD STRENGTH, (Oe)

The observed satellite intensities are 0.094:0.27:0.67:2.0:3.3:16: 3.3:2.0:0.67:0.27:0.094 as the relative intensities of the two shoulders, the satellite lines, and the central line. These are the relative amplitudes of the peaks on the absorption spectrum. The satellites are about three times as intense as compared with the central line as in the case of scandium metal (30).

The Knight shifts for the Mn nuclei were calculated with respect to an nmr frequency of 10.500 MHz in a 10 KOe field for the free ^{55}Mn ion. In accordance with the recently revised ^{55}Mn moment value (31).

The nmr spectrum of $ScMn_2$ was also investigated at 77°K and at 4°K. There was no change in K_{iso} of the Sc. The line position was the same to within $\pm$0.008% of the total value of the field. The quadrupole frequency ν_Q of ^{45}Sc is 3.9$\pm$1.1 KHz larger at both 77°K and 4°K. Any change between the two temperatures is less than 2 KHz. So ν_Q=59.4 KHz at 77°K and 4°K, while it is 55.5 KHz at room temperature, according to table 2.

The K_{iso} of the symmetrical Mn is unchanged from room temperature at the lower temperatures to within 0.008%. The quadrupole frequency of the symmetrical Mn in increased 2.6 $\pm$ 0.4% at 77°K and 3.3 $\pm$ 0.4% at 4°K from that at room temperature.

The position of the asymmetrical Mn resonance decreased 0.023$\pm$0.020% of the total field at the lower temperatures with no significant difference between the temperatures. This makes K_{iso}= 0.67% at 77°K and 4°K as compared with K_{iso}= 0.69% at room temperature from table 2. Except for the shift of the entire spectrum, due to the change in Knight shift, the lines kept the same positions to within 0.02% of the entire interaction. There were no measurable changes in the other parameters with temperature.

These resonance parameters and their small variation with temperature are not unexpected for $ScMn_2$.

2. $\underline{ErMn_2}$

The parameters of the room temperature nmr resonance of $ErMn_2$ are shown on table 3. There is very little change on going to liquid nitrogen temperature. For Mn_I, at 77°K, the positively shifted line is 0.0425±0.055% of the entire field above the position of the line at room temperature and the negatively shifted line is 0.085±0.04% of the entire field below the line position at room temperature. These data were taken at 13 and 14 MHz. The shifts are so small and uncertain that it is difficult to tell which resonance parameter has changed. If all the shift were caused by a change in the quadrupole coupling, the quadrupole frequency ν_Q would increase 16±12 KHz. If the entire change were due to a change in the Knight shift, the isotropic Knight shift would decrease 0.03% and the axial component of the Knight shift would decrease 0.07%. These are both less than the probable errors in the room temperature data.

For Mn_{II} a few lines have been studied in detail at 77°K. The line with the lowest effective gamma in the spectrum, which Narita et al. (21) call y_{22} has a shift of +0.06±0.06% of the entire field at liquid nitrogen temperature from the value at room temperature at 13 MHz. The most prominent line in the spectrum, which Narita calls y_{13} has no shift at liquid nitrogen temperature ±0.06% at 13 MHz. The line with the highest effective gamma in the spectrum has a Knight shift +0.02 ± 0.05% higher at liquid nitrogen temperature than at room temperature.

It appears that any changes in the resonance parameters between room temperature and liquid nitrogen temperature are at most 0.06%. The changes

Table 3. Summary of the Knight shift and quadrupole coupling parameters for the ^{55}Mn resonance spectra in $ErMn_2$ (at $300^{o}K$)

	$^{55}Mn_{I}$	$^{55}Mn_{II}$
Site Symmetry	$\bar{3}m$	mm
K_{iso}(%)	0.58 ± 0.06	0.34 ± 0.2
K_{ax}(%)	0.06 ± 0.07	-0.07 ± 0.1
K_{aniso}(%)	0	-0.023 ± 0.05
ν_Q(MHz)	2.77 ± 0.05	2.00 ± 0.18
e^2qQh^{-1}(MHz)	18.4 ± 0.3	13.3 ± 1.2
η	0	0.36 ± 0.10

are so small that almost nothing can be said about changes in the actual parameters. One might say that the K_{iso} increased 0.025% to 0.36% and ν_Q increased 0.022% to 2.04 MHz. All the changes between the room temperature and liquid nitrogen temperature are less than the experimental error at room temperature.

3. $\underline{TmMn_2}$

The parameters of the room temperature nmr spectrum of $TmMn_2$ are shown on Table 4. As in the cases of the other two compounds, there is

Table 4. Summary of the Knight shift and quadrupole coupling parameters for the ^{55}Mn resonance spectra in $TmMn_2$ (at 300°K)

	$^{55}Mn_I$	$^{55}Mn_{II}$
Site symmetry	$\bar{3}m$	mm
K_{iso}(%)	0.9 ± 0.2	0.56 ± 0.10
K_{ax}(%)	-0.2 ± 0.2	0.03 ± 0.05
K_{aniso}(%)	0	0.03 ± 0.1
ν_Q(MHz)	2.8 ± 0.2	2.24 ± 0.22
e^2qQh^{-1}(MHz)	18.8 ± 1.3	14.9 ± 1.5
η	0	0.39 ± 0.14

very little change in the $TmMn_2$ spectrum with temperature. The most prominent line in the spectrum is that called ν_3 by Baugher and ν_{13} by Narita. It is detectable at 77°K with our equipment and has shifted less than 0.01% of the total field. Thus, for example, if this change were due entirely to a change in the isotropic Knight shift, the latter would change by this amount. From this result, it is expected that the parameters for both symmetry positions do not change significantly, since the position

of this line is determined by the x and y Knight shifts, the quadrupole coupling, and the asymmetry parameter, η. The resonance parameters for the asymmetric nuclear site should be affected by the same factors which affect the symmetric site, so that since the parameters remain constant for the asymmetric site, they should remain constant for the symmetric site also. The $TmMn_2$ spectrum was rather difficult to resolve at $77^{o}K$ due to the small amount of sample allowed in the dewar and other factors.

B. Magnetic Susceptibility Results

1. $ScMn_2$

The magnetic susceptibility of $ScMn_2$ is $+0.48 \times 10^{-6}$ emu/g or 74×10^{-6} emu/gram formula weight at room temperature. The susceptibility is not expected to change significantly with temperature because of the electronic structure of Sc and because Mn has been found to have no magnetic moment in these compounds of this structure (32).

2. $ErMn_2$

Measurements here of the magnetic susceptibility of $ErMn_2$ from $77^{o}K$ to $296^{o}K$ showed a $p_{eff} = 9.56 \pm 0.03$ Bohr magnetons and a ferromagnetic ordering temperature of $14 \pm 1^{o}K$. This is very close to the effective magneton number experimentally determined for the Er^{+3} ion (4) which is 9.5. A previous measurement by Kirchmayr (33) in the same temperature range and up to $1600^{o}K$ yielded an antiferromagnetic ordering temperature of $-90^{o}K$ and an effective magnetic moment of 10.1 Bohr magnetons. His error limits are not given, but contamination by Er_6Mn_{23} is mentioned in the text. Actually, ferromagnetic coupling is observed (32) and the comment by Kirchmayr that the antiferromagnetic coupling corresponds to a ferromagnetic coupling of the Er moments and antiparallel coupling of small Mn moments does not

seem to be valid since Felcher (32) measured no average Mn magnetic moment along the direction of magnetization. Mössbauer work also indicates that there is probably no magnetic moment on the Mn in these compounds (34).

3. $\underline{TmMn_2}$

Measurements here of the magnetic susceptibility of $TmMn_2$ from $77^{o}K$ to $297^{o}K$ showed a $p_{eff} = 7.64 \pm 0.05$ Bohr magnetons and a ferromagnetic ordering temperature of $3.3 \, {}^{+7}_{-1.4} \, {}^{o}K$. This is very close to the effective magneton number experimentally determined for the Tm^{+3} ion (4) which is 7.3. $TmMn_2$ was found to be ordered at $4.2^{o}K$ by Felcher (32).

C. Electric Field Gradient Calculations and Discussion

Table 5 summarizes the calculations of the electric field gradient at the nucleus, due to the surrounding ions in the lattice, by the DeWette method (15). The ion positions used were the same as those used by Uhrich, et al. (34). The lattice parameters were $a = 5.033$ Å, $c = 8.278$ Å, $\alpha = 1.6447$ for $ScMn_2$; $a = 5.281$ Å, $c = 8.621$ Å, and $\alpha = 1.6325$ for $ErMn_2$; and $a = 5.24$ Å, $c = 8.565$ Å, and $\alpha = 1.6342$ for $TmMn_2$ where $\alpha = c/a$.

The program used for these calculations and some discussion of them will be found in Appendix A. Inclusion of a larger number of terms in these calculations than had been used formerly may explain the difference between these numbers and those implied in reference 34.

The electric field gradients due to each ion at a particular site are presented separately, so they may be considered independently. These are the gradients due to the surrounding ions, but not due to the closed electron shells of the ion. If V_{zz} is the field gradient at the nucleus due to the other ions in the material, including the antishielding due to the closed electron shells of the ion,

Table 5. Electric field gradient (V'_{zz}/e) by the DeWette method due to each ion on the various ion sites ($\times 10^{24}$ cm^{-3}). See reference 15

	R^{+3} (Rare Earth) at R	R^{+3} at Mn_I	R^{+3} at Mn_{II}	Mn^{+2} at Mn_I	Mn^{+2} at Mn_{II}	Mn^{+2} at R
$ScMn_2$	0.002221	-0.4787	0.1503	1.331	1706	-0.01395
$ErMn_2$	-0.003269	-0.4231	0.1196	0.7782	984.5	-0.008776
$TmMn_2$	-0.004088	-0.4332	0.1227	0.7948	1008.	-0.008858

$$V_{zz} = V_{zz}'(1 - \gamma_\infty),$$

as explained in the section on the electric field gradient calculation.

In order to calculate the effective charge on the Mn ions and the effective Sternheimer antishielding factor for the Mn, we will consider the equation

$$\left[\frac{3\, e^2 Q |(1 - \gamma_\infty)|}{2I(2I-1)h}\right]\left[(V_{zz}'/e)_{R^{+3}\text{ at Mn}} + x(V_{zz}'/e)_{Mn^{+2}\text{ at Mn}}\right] = \nu_Q$$

where ν_Q is the measured quadrupole frequency found in tables 2, 3, and 4, Q is the nuclear quadrupole moment, I is the nuclear spin, γ_∞ is the Sternheimer antishielding factor, and V_{zz}' is the calculated electric field gradient, found in Table 5. The equation will be solved for $(1 - \gamma_\infty)$ and x. 2x is the effective charge on the Mn ions, in units of -e. In Table 5 and in this equation, the electric field gradients are considered to be those due to rare earth ions of charge -3e and Mn ions with charge -2e.

The best fit of this equation with the six measured quadrupole frequencies at the Mn sites yields $x = 0.00015 \pm 0.00007$. This says that Mn has an effective charge of -0.0003 e, making the assumptions implicit in the DeWette sum calculation, including that of no conduction electron shielding. However, electron shielding would increase the effect of the Mn ions, since the nearest neighbors of the rare earth ions are twelve Mn ions. These are followed by four R ions only slightly further away. The next nearest neighbor grouping contains fifteen Mn ions and six R ions. One must conclude with Uhrich et al. (34) that in these compounds Mn carries an effective charge of zero.

The best fit of the equation to the data also yields $|(1 - \gamma_\infty)| = 0.8$

where Q is taken as 0.6×10^{-24} cm^2 for ^{55}Mn (35). The largest uncertainty is in the value of Q. Alternatively, one can in the same way extract a value of $|(1 - \gamma_\infty)|Q$ from the experimental data, yielding $(0.463 \pm 0.009) \times 10^{-24}$ cm^2 for Mn_I and $(0.46 \pm 0.1) \times 10^{-24}$ cm^2 for Mn_{II}. The values are identical, within the limits of error.

The effective charges were assumed to be the same for both ion sites, since both have hyperfine fields which are independent of temperature and for convenience in the De Wette calculation. The DeWette calculation could have been partitioned into contributions from the two separate sites but this was not done. The two sites yield the same Sternheimer antishielding factor, assuming the same effective charge for the Mn ion on each site. This calculation assumes no conduction electron shielding.

There is another method for calculating the Sternheimer antishielding factor for Mn. A ratio of the Sternheimer antishielding factors of Sc and Mn may be found from the measured quadrupole frequencies and the calculated electric field gradients.

$$\frac{\nu_{Q\ Sc}}{\nu_{Q\ Mn}} = \frac{\{[Q/I(2I-1)](1 - \gamma_\infty)V'_{zz}\}_{Sc}}{\{[Q/I(2I-1)](1 - \gamma_\infty)V'_{zz}\}_{Mn}} ,$$

This equation can be turned around to yield the following equation

$$\left| \frac{(1 - \gamma_\infty)_{Sc}}{(1 - \gamma_\infty)_{Mn}} \right| = \frac{(Q\ V'_{zz}(calc)/I(2I-1))_{Mn}\ \nu_{Q\ Sc}}{(Q\ V'_{zz}(calc)/I(2I-1))_{Sc}\ \nu_{Q\ Mn}}$$

Q will be taken as -0.22×10^{-24} cm^2 for ^{45}Sc (35). The ratio of $|(1 - \gamma_\infty)_{Sc}/(1 - \gamma_\infty)_{Mn}|$ is 22. Using $\gamma_\infty = -7$ for Sc^{+3}, then $|(1 - \gamma_\infty)|$

for the Mn in these compounds, averaged over the three compounds, is 0.37. The chief uncertainty again is in the value of the nuclear quadrupole moment for Mn. $|(1 - \gamma_\infty)|Q$ for Mn is 0.22×10^{-24} cm^2 with the chief uncertainty in the quadrupole moment of Sc or the Sternheimer factor for Sc. There appears to be very little shielding by the electron shells of the Mn ion. The assumption that the conduction electron shielding is the same for both nuclear species is implied in the derivation of this equation. This does not seem unreasonable for two species in one compound and even extrapolation to this family of compounds is reasonable. The two calculations of the Sternheimer factor differ by a factor of two. This may be due to conduction electrons or an error in the Q or $(1-\gamma_\infty)$ for Sc.

D. Conclusions from the Knight Shift and Susceptibility Results

The susceptibility of the rare earth compounds studied here is inversely proportional to the temperature, but the Knight shifts do not depend on the temperature. In these compounds, $K_f(T)$ of equation 8 is zero. Either there is essentially no interaction between the 4f electrons and the Mn nuclei, or the interaction is compensated by some other effect.

Another indication that there is no interaction between the 4f electrons in the rare earth ions and the Mn nuclei is the similarity between the Knight shifts of the Mn nuclei in $ScMn_2$ and those in the compounds with the rare earth ions. The Mn_I isotropic Knight shift in $ScMn_2$ is 0.9%; in $TmMn_2$ it is also 0.9%; and in $ErMn_2$ it is 0.58%. The Mn_{II} isotropic Knight shift is 0.69% in $ScMn_2$, 0.56% in $TmMn_2$ and 0.34% in $ErMn_2$.

There is a substantial temperature independent Knight shift in $ErMn_2$

and $TmMn_2$ and no temperature dependence of the Knight shift. This is strikingly different from the case of the rare earth intermetallic compounds with Sn (36, 37), Al (38, 39), P, As, Sb, and Bi (10), all those that have been studied heretofore. This is also different from the case of the beryllium-based Laves phase intermetallic compounds, (40), and V_3X compounds investigated by Clogston and Jaccarino (41) and discussed by Bennett et al. (42), and Nb_3Sn (43, 44).

In almost all the other compounds there is communication between the rare earth or transition metal ion and the nucleus of the other element via the conduction electrons. This does not seem to be the case in the Mn compounds studied here.

The reason for this may be that the Mn nuclei have no contact with the conduction electrons. The outer d electrons of the Mn may form a band well below the Fermi surface. This could accommodate the finding of zero magnetic moment on the Mn ion by Felcher et al. (32). The detailed distribution of the electrons in the band could concentrate them at the Mn sites so that the electrons closer to the Fermi surface would have a small probability of being at the Mn nuclear sites. A similar conclusion was reached independently by Uhrich et al. (34) who say their results could be accounted for in terms of a highly localized band picture for the Mn ion in which no net spin polarization of the band occurs.

This occurrence of a metal nucleus having almost no contact with the conduction band is well documented for another, quite different, type of compounds, the metal tungsten bronzes (45, 46, 47).

Another intermetallic compound with a Knight shift independent

of temperature for one of the components is CoAl with the Al Knight shift temperature independent (48, 49, 50). Seitchik concluded that there is little Al s-character in the Fermi surface states of CoAl.

In the case of the metal tungsten bronzes, the Knight shift for Li, Na and Tl in the tungsten bronze have been found to be extremely small (47). This was one of the indications that there was no contact with the conduction band in these cases. In the case of CoAl, the measured Knight shift of the Al is 0.014% (50), and yet the Al Knight shift is independent of temperature even though the Co Knight shift and the susceptibility depend on temperature. In the compounds studied here, there are Knight shifts of up to 0.9% for the Mn resonances. These shifts may be caused by the orbital contribution to the Knight shift, expressed in equation 4. According to Bennett, et al. (42) particularly strong orbital effects are expected in roughly half-filled d-band transition metals.

Another case of Knight shifts being independent of temperature in the same material with others which are temperature dependent is α - Mn. It has four crystallographically inequivalent sites. Two have temperature dependent Knight shifts with one of those peaking at the temperature at which the susceptibility peaks. The two other sites have temperature independent Knight shifts (51, 52)

The possibility in the case of the RMn_2 compounds of a simple node in the conduction electron wave function at the Mn nuclei such as Keller(53) suggested for the tungsten bronzes seems quite unlikely because there are two different sites for the Mn nuclei and there would have to be nodes at both sites to yield the observed results.

The other possibility of an occurrence of a node, that the RKKY

spin polarization has a zero value at the nuclei in question also seems quite unlikely because of the two different sites.

Another possibility that can be discarded is that the conduction electrons which are polarized are in the d state. If this were the case, there would be a temperature dependent core polarization contribution to the Knight shift, and the Knight shift would still be temperature dependent.

The samples are metallic. They have a typical metallic luster and they are good conductors of electricity as measured by a lab ohm meter, so there must be conduction electrons. We can discard the possibility that there are no conduction electrons to transmit the rare earth ion magnetization to the Mn.

It could be that for some reason peculiar to the structure type that there is no polarization of the conduction electrons. This is hard to believe because the structure is so close to the cubic Laves phase compounds (54) in which polarization has been observed (38) and the compounds do order ferromagnetically. There must be polarization of the conduction electrons to transmit the magnetic information from one rare earth ion to another.

In conclusion, it seems that another rather rare case of a nuclear component in an intermetallic compound which does not communicate with the conduction band has been found in the case of Mn in the hexagonal Laves phase compounds $ScMn_2$, $ErMn_2$, and $TmMn_2$. This element occupies two sites in the compound. In other words, $\langle |\psi(0)|^2 \rangle$ averaged over the Fermi surface, as defined in equation 1, is zero at both Mn sites. Also, $\langle |\phi_{core}(0)|^2 \rangle$ as defined in equation 2 is zero.

V. REFERENCES

1. Knight, W. D., Electron Paramagnetism and Nuclear Magnetic Resonance in Metals, Solid State Physics, Vol. 2, Seitz and Turnbull, eds. Academic Press, New York, 1956, Pp. 93-136.

2. Jaccarino, V., Studies of the Hyperfine Interaction in Transition Metals, W. Marshall, ed., Theory of Magnetism in Transition Metals, Academic Press, New York and London (1967).

3. Slichter, Charles P., Principles of Magnetic Resonance, Harper and Row, New York, N. Y. (1963).

4. Kittel, Charles, Introduction to Solid State Physics, Second Edition, John Wiley and Sons, Inc. New York (1953).

5. Narath, Albert, Nuclear Magnetic Resonance in Magnetic and Metallic Solids, Arthur J. Freeman and Richard B. Frankel, eds., Hyperfine Interactions, Academic Press, New York and London, (1967).

6. Jaccarino, V., B. T. Matthias, M. Peter, H. Suhl, and J. H. Wernick, Phys. Rev. Letters, 5, 251 (1960).

7. Jaccarino, V., J. Appl. Phys. 32, 102S (1961).

8. Yosida, K., Phys. Rev. 106, 893 (1957).

9. Doniach, S., Conduction-Electron Localized Moment Interaction in Rare-Earth Metals and Dilute Alloys, W. Marshall, ed., Theory of Magnetism in Transition Metals, Academic Press, New York and London (1967).

10. Jones, E. D., Phys. Rev. 180, 179 (1969).

11. Abragam, A. The Principles of Nuclear Magnetism, Oxford, London (1961).

12. Barnes, R. G. and B. K. Lunde, J. Phys. Soc. Japan 28, 408 (1970).

13. Schratter, J. J. and D. L. Williams, Phys. Let. 26A, 79 (1967).

14. Jones, W. H. Jr., T. P. Graham, and R. G. Barnes, Phys. Rev., 132, 1898 (1963).

15. DeWette, F. W., Phys. Rev. 123, 103 (1951).

16. Sternheimer, R. M., Phys. Rev. 130, 1423 (1963).

17. Das, T. P., and M. Pomerantz, Phys. Rev. 123, 2070 (1961).

18. Uhrich, D. L. and R. G. Barnes, Phys. Rev. 164, 428 (1967).

19. Das, K. C. and D. K. Ray, Phys. Rev. 187, 777 (1969).

20. Low, W., Solid State Phys. Suppl. 2, 57 (1960).

21. Narita, K., J. Umeda, and H. Kusumoto, J. Chem. Phys., 44, 2719 (1966).

22. Baugher, J. F., P. C. Taylor, T. Oja, and P. J. Bray, J. Chem. Phys., 50, 4914 (1969).

23. Bloch, F., Phys. Rev. 70, 460 (1946).

24. Torgeson, D. R., Rev. of Sci. Instr. 38, 612 (1967).

25. Torgeson, D. R., U. S. Atomic Energy Commission Report IS-1312 [Ames Lab., Ames, Iowa] (1965).

26. Lecander, R. G., A Study of the Effects of Impurities and Vacancies on Nuclear Magnetic Resonance Line Shapes in Intermetallic Compounds, unpublished Ph.D. thesis, Library, Iowa State University, Ames, Iowa (1967).

27. Creel, R. B., Nuclear Magnetic Resonance in Transition Metal Borides, unpublished Ph.D. thesis, Library, Iowa State University, Ames, Iowa (1969).

28. Selwood, Pierce W., Magnetochemistry, 2nd ed., Interscience Publishers, New York, (1956).

29. Adams, J. E., B. F. Williams, and R. R. Hewitt, Phys. Rev. 151, 238 (1966).

30. Barnes, R. G., F. Brosa, S. L. Segal, and D. R. Torgeson, Phys. Rev., 137, A1828 (1965).

31. Mims, W. B., G. E. Devlin, S. Geschwind and V. Jaccarino, Phys. Letters 24A, 481 (1967).

32. Felcher, G. P., L. M. Corliss, and J. M. Hastings, J. of Appl. Phys. 36, 1001 (1965).

33. Kirchmayr , Hans R. IEEE Trans. on Magnetics, Mag-2, 493 (1966).

34. Uhrich, D. L., D. J. Genin, and R. G. Barnes, Phys. Rev. 166, 261 (1968).

35. Varian Associates, Nuclear Magnetic Resonance Table, fifth edition.

36. Barnes, R. G., F. Borsa, and D. Peterson, J. Appl. Phys. 36, 940 (1965).

37. Borsa, F., R. G. Barnes, and R. A. Reese, Phys. Stat. Sol. 19, 359 (1967).

38. Jaccarino, V., B. T. Matthias, M. Peter, H. Suhl, and J. H. Wernik, Phys. Rev. Letters, 5, 251 (1960).

39. Jaccarino, V., J. Appl. Phys. 32, 102S (1961).

40. Saji, M., T. Yamadaya and M. Asanuma, J. Phys. Soc. Japan, 21, 255 (1966).

41. Clogston, A. M. and Jaccarino, V., Phys. Rev. 121, 1357 (1961).

42. Bennett, L. H., R. E. Watson, and G. C. Carter, Relevance of Knight Shift Measurements to the Electronic Density of States, presented at the Electronic Density of States Symposium, National Bureau of Standards, Washington, D.C., November, 1969.

43. Shulman, R. G., B. J. Wylunda, and B. T. Matthias, Phys. Rev. Letters 1, 278 (1958).

44. Lutgenmeier, M., Z. Naturforsch, 20A, 246 (1965).

45. Karian, H. G., Tight Binding Energy Bands of Perovskite Type Transition Metal Oxides, unpublished Ph.D. thesis, Library, Iowa State University of Science and Technology, Ames, Iowa (1969).

46. Fromhold, A. T., Jr., and Albert Narath, Phys. Rev. 152, 585 (1966).

47. Jones, W. H., Jr., E. A. Garbaty, and R. G. Barnes, J. Chem. Phys. 36, 494 (1962).

48. West, G., Phil. Mag. 9, 979 (1964).

49. West, G., Phil. Mag. 15, 855 (1967).

50. Seitchik, J. A., and R. H. Walmsley, Phys. Rev. 137, A143 (1965).

51. Seitchik, J., V. Jaccarino, and J. H. Wernick, Bull. Am. Phys. Soc. 10, 317 (1965).

52. Andersson, L. O., Phys. Letters 26A, 279 (1968).

53. Keller, J. M., J. Chem. Phys. 33, 1231 (1960).

54. Gschneidner, K. A., and W. B. Pearson, Mat. Res. Bull., 3 951 (1968). Pergamon Press, inc., U.S.A.

VI. ACKNOWLEDGEMENTS

I wish to thank Dr. R. G. Barnes for his helpful suggestions, constructive criticism and guidance during the course of this investigation.

I would like to thank Mr. D. R. Torgeson, who designed and built one of the nmr spectrometers and the continuous averaging equipment; Mr. R. D. Schmidt and Mr. B. J. Beaudry who prepared the samples; and Mr. J. D. Greiner, who made available the equipment for measuring magnetic susceptibilities and made most of the susceptibility measurements.

I would also like to thank my husband, Paul, and my parents, Dr. and Mrs. Roy Kegerreis for their continuing encouragement and my baby sitter, Mrs. Hannah Berhow, for her invaluable help during this time.

VII. APPENDIX A

This section contains the listings of the Fortran computer program that was used to do the DeWette sums (15). In experimenting with the program, it was found that a sum considering a plane 35 atoms square is required for accuracy.

In the sums done for Sc in $ScMn_2$, assuming the Sc and Mn ions to have charge of +3, and the compound to have an α of 1.63299, for instance, sums with 35, 37, and 57 terms in the De Wette sum yielded values constant to within 0.3%, while sums with 21 and 23 terms were 50% different from each other and the average was 15% different from the sums with more terms. The suns for 15 and 17 terms were different by a factor of 150. The sum for 17 terms was only 1/32 of the sum with 35 terms. 17 terms is the standard number that has been used in these calculations in the past and this may account for any differences from previously published results. The sum considered here was that for $(V'_{zz}/e)_{Sc^{3+}}$ at Mn_{II}.

```
C      PROGRAM DWS(DEWETTE SUMS)
C
C      THIS PROGRAM WILL CALCULATE THE DEWETTE SUMS FOR A TETRAGONAL OR
C      HEXAGONAL CRYSTAL.  THE SUM IS FOUND IN PHYSICAL
C      REVIEW, 123, 103, (1961).
C
C      INPUT DATA:
C                      A = BASAL LATTICE VECTOR.
C                      C = LATTICE VECTOR PERPENDICULAR TO BASAL PLANE
C                      XV = VOLUME OF ONE ION.
C                      NS = NUMBER OF SUMS TO BE DONE (ONE CORRESPONDING TO
C                           EACH ATOM IN THE UNIT CELL).
C                      L IS 1 FOR TETRAGONAL LATTICE, ZERO FOR HEXAGONAL
C                           LATTICE.
C                      X1, X2, X3 ARE ION COORDINATES IN FRACTIONAL LATTICE
C                           CONSTANTS.
C                      Z = CHARGE ON THE ION.
C                      Z1 = CHARGE GIVEN TO THE CONDUCTION BAND PER ION
C
      DIMENSION TITLE(20),SS(20)
      DATA XS3/.8660255/
C
  300 READ (1,1)(TITLE(I),I=1,20)
      READ(1,2) A,C,    XV,Z,Z1,NS,L
      IF(NS.LE.0)STOP
   20 ALPHA=C/A
      WRITE (3,4) (TITLE(I),I=1,20)
      IF (L .EQ. 0) XO=XS3
      IB=0
      XV=XO*XV*A*A*C
      XQ = 0.0
      DO 200 N=1,NS
      READ (1,3) X1,X2,X3
      IF (X1 .EQ. 0. .AND. X2 .EQ. 0. .AND. X3 .EQ. 0.) IB=1
      S=0.0
      SS(N)=0.0
C
```

```
C          DO THE DOUBLE SUM ON MU(1) AND MU(2).
       DO 100 I=1,35
       DO 100 K=1,35
C
C          CALCULATE THE DISTANCE OF THE ICN FROM THE Z AXIS.
       IF(L.GT.0)GO TO 60
    50 R=SQRT(4.*(FLOAT((I-18)**2)-FLOAT((I-18)*(K-18))
      C+FLOAT((K-18)**2))/3.)
       GO TO 70
    60 R=SQRT(FLOAT((I-18)**2)+FLOAT((K-18)**2))
    70 CONTINUE
       IF(R.LE.0)GO TO 130
C
C          CALCULATE THE ARGUMENTS OF THE TRANSCENDENTAL FUNCTIONS.
       E=-2.*3.1415927*(FLOAT(I-18)*X1+FLOAT(K-18)*X2)
       F1=2.*3.1415927*R*ALPHA*(1.-X3)
       F2=2.*3.1415927*R*ALPHA*X3
       D1=2.*3.1415927*R*ALPHA
       IF(X1 .EQ. 0 .AND. X2 .EQ. 0 .AND. X3 .EQ. 0) GO TO 80
    90 F=EXP(-F1)+EXP(-F2)
       D=1.-EXP(-D1)
       GO TO 120
    80 IF (D1. GT. 174.673) D1 = 174.6
       D=EXP(D1) - 1.
       F = 2.0
   120 CONTINUE
C
C          CALCULATE THE INDIVIDUAL TERMS OF THE SUM AND COMBINE.
       B=COS(F)
       SS(N)=SS(N)+B*F*R/D
       GO TO 130
   130 CONTINUE
   100 CONTINUE
       S=(4.*3.1415927**2/(XO*A**3))*SS(N)*Z
       WRITE (3,5) X1,X2,X3,S
       XQ=XQ+S
   200 CONTINUE
```

```
C
C        CALCULATE Q(LATTICE).
      IF(L.GT.0)GO TO 40
   30 BETA=-11.0341754
      GO TO 110
   40 BETA=-9.0336217
  110 XA=Z1*8.*3.1415927/(3.*XV)
      IF (IB .EQ. 0) BETA=0.
      XB=Z*BETA/A**3
      XQ=XQ+XA+XB
      WRITE (3,6) XQ
      GO TO 300
    1 FORMAT (20A4)
    2 FORMAT (5F10.4,2I5)
    3 FORMAT (3F10.4)
    4 FORMAT (1H1,20A4)
    5 FORMAT (8H0      S(,F6.4,1H,,F6.4,1H,,F6.4,4H) = ,E16.8)
    6 FORMAT (1H0,17H      Q(LATTICE) =,E16.8)
      END
```

VIII. APPENDIX B

This section contains a summary of the analytical results of Baugher et al. (22) and Narita et al. (21) which are used in this thesis. Table 6 is a table of the frequency of the shoulders and singularities in the powder pattern for the $m = \frac{1}{2} \rightarrow -\frac{1}{2}$ transition for a nucleus in a position without axial symmetry. It is part of Table 1 of Baugher et al. The numbered ν's are the labels given to each shoulder or singularity. ν_o is the resonance frequency of the isolated nucleus. $R = \nu_Q^2(I(I + 1) - 3/4)$. $\eta = (V_{xx} - V_{yy}) / V_{zz}$. The σ's are used to designate the chemical shift. This is the same phenomon as the Knight shift in metals, except for sign. $3\ K_{iso} = -(\sigma_1 + \sigma_2 + \sigma_3)$, $6\ K_{ax} = -2\ \sigma_3 + \sigma_1 + \sigma_2$, and $2\ K_{aniso} = \sigma_3 - \sigma_2$.

Table 7 is a table of the frequency of the shoulders and singularities in the powder pattern for the $m = \frac{1}{2} \rightarrow -\frac{1}{2}$ transition for a nucleus in a position without axial symmetry and with no Knight or chemical shift. It is assembled from equations 10, 12, and 13 of Narita , et al. (21) The correct equation for y is

$$y = -\nu / \{(\nu_Q^2/6\ \nu_o)\,[I(I+1) - 3/4]\}.$$

Figure 3 is the line shape function G(Y) for the case of $\eta = 0.6$. Positions of y_{11}, y_{12}, etc. were determined from the equations in Table 7 This figure is adapted from Narita et al. (21). The data reported herein resembled this figure because the anisotropy in the Knight shift is rather small for these compounds. G(y) is the frequency that y lies between y and $y + \Delta y$ for every angular direction which could be chosen corresponding to lattice points on a sphere equally divided by area. In effect, G(y) represents the relative resonance intensity in the interval y to $y + \Delta y$.

Table 6. Frequency in the presence of quadrupolar and chemical shift effects of shoulders and singularities in powder pattern for $m = \frac{1}{2} \rightarrow -\frac{1}{2}$ transitions. This is part of Table 1 of Baugher (22)

$$\nu_1 = \nu_0 + [R(3 + \eta)^2 / 144\,\nu_0] - \sigma_1\nu_0$$

$$\nu_2 = \nu_0 + [R(3 - \eta)^2 / 144\,\nu_0] - \sigma_2\nu_0$$

$$\nu_3 = \nu_0 + \frac{R(1 - \eta^2)}{18\nu_0} - \frac{1}{2}[1 + (3\eta)^{-1}]\sigma_2\nu_0 - \frac{1}{2}[1 - (3\eta)^{-1}]\sigma_1\nu_0 - \frac{(\sigma_2 - \sigma_1)^2\nu_0^3}{\eta^2 R}$$

$$\nu_4 = \nu_0 + [R\eta^2 / 36\nu_0] - \sigma_3\nu_0$$

$$\nu_5 = \nu_0 - \frac{R(1 - \eta)}{9\nu_0} - \frac{(5 - \eta)\sigma_3 + 2(2 - \eta)\sigma_1}{3(3 - \eta)}\nu_0 - \frac{4(\sigma_3 - \sigma_1)^2\nu_0^3}{(3 - \eta)^2 R}$$

$$\nu_6 = \nu_0 - \frac{R(1 + \eta)}{9\nu_0} - \frac{(5 + \eta)\sigma_3 + 2(2 + \eta)\sigma_2}{3(3 + \eta)}\nu_0 - \frac{4(\sigma_3 - \sigma_2)^2\nu_0^3}{(3 + \eta)^2 R}$$

Table 7. Frequency in the presence of quadrupolar effects of shoulders and singularities in power pattern for $m = \frac{1}{2} \rightarrow -\frac{1}{2}$ transitions

$$y_{11} = -3/8 - (1/4)\eta - (1/24)\eta^2$$

$$y_{12} = -(3/8) + (1/4)\eta + (1/24)\eta^2$$

$$y_{13} = -1/3 + (1/3)\eta^2$$

$$y_{21} = 2/3 - (2/3)\eta - (1/54)\eta^2$$

$$y_{22} = 2/3 + (2/3)\eta - (1/54)\eta^2$$

$$y_z = -(1/6)\eta^2$$

Figure 3 . Line shape function G(y) for $\eta = 0.6$ and isotropic Knight shift. Figure adopted from reference 21

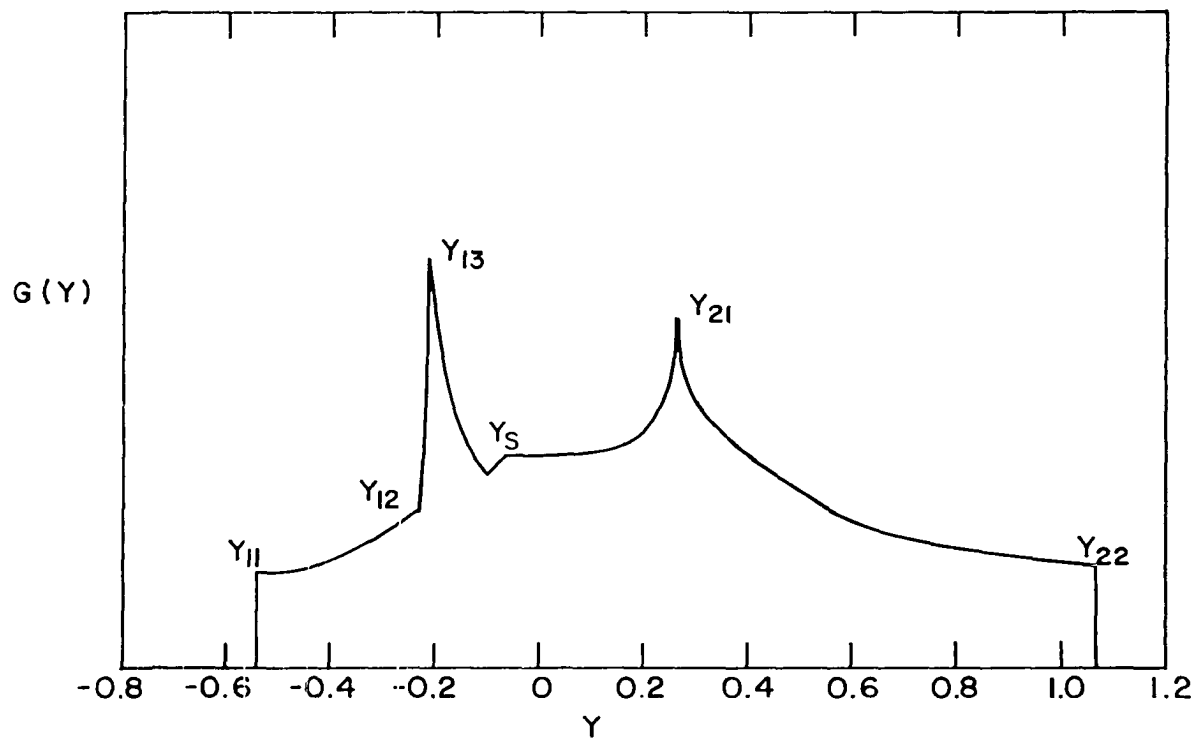
G(Y)
Y13
Y21
YS
Y12
Y11
Y22
-0.8
-0.6
-0.4
-0.2
0
0.2
0.4
0.6
0.8
1.0
1.2
Y

IX. APPENDIX C

This appendix contains the listings of the Fortran computer program that was used to calculate the line position and other parameters for each resonance line. A sample of the print out for one short example is also included.

```
C      PROGRAM FOR CALCULATION OF LINE POSITION FROM RAW DATA
C
C      INPUT DATA:
C                F0 = RF FREQUENCY ON SAMPLE
C                F1 = FREQUENCY OF FIRST CALIBRATE RESONANCE IN MHZ
C                P1 = POSITION OF FIRST CALIBRATE RESONANCE
C                PX = POSITION OF DATA POINT X
C                RGAMMA = GYROMAGNETIC FREQUENCY OF REFERENCE ELEMENT
C                SGAMMA = GYROMAGNETIC FREQUENCY OF SAMPLE ELEMENT
C                NL = NUMBER OF SAMPLE LINES TO CALCULATE
C      FIRST DATA CARD HAS GAMMA OF REFERENCE IN 1ST 10 SPACES,
C      THEN GAMMA OF SAMPLE IN NEXT 10 SPACES (START WITH SPACE 11),
C      THEN FREQUENCY OF DATA IN NEXT 10 SPACES (START WITH SPACE 21),
C      THEN THE TOTAL NUMBER OF LINES IN NEXT 10 SPACES (START WITH 31)
C      SECOND DATA CARD HAS CALIBRATION FREQUENCIES, START WITH 1 AND 11
C      THIRD DATA CARD HAS CALIBRATION POSITIONS, START WITH 1 AND 11
C      FORTH DATA CARD HAS THE LINE NUMBER IN 1ST 10 SPACES, THEN
C      LINE POSITION IN SECOND 10.  ALWAYS USE DECIMAL POINTS.
       DIMENSION TITLE (20)
       REAL    IVOESQ, KEFF, IVFRS
  300  READ (1,1,END=200) (TITLE(I),I=1,20)
       READ (1,2) RGAMMA, SGAMMA, F0, NL
       READ (1,3) F1, F2
       READ (1,3) P1, P2
       WRITE (3,4) (TITLE(I),I=1,20)
C       CALCULATE SQUARE AND INVERSE SQUARE OF FREQUENCY
       FRESQ = F0**2
       WRITE (3,7) F0,FRESQ
       IVFRS = 1./ FRESQ
       WRITE (3,12) IVFRS
C       CALCULATE NUMBER OF HZ AND OE PER CHART LINE
       DRP = P2- P1
       DRF = F2- F1
       HZPL = DRF/DRP
       OEPL = (HZPL/RGAMMA)*10000.
       WRITE (3,13) HZPL, OEPL
C       CALCULATE EFFECTIVE GAMMA, KNIGHT SHIFT, MAGNETIC FIELD
```

```
C       AND INVERSE OF THE MAGNETIC FIELD SQUARED FOR EACH LINE
      OER = (F1/RGAMMA)* 10000.
      DO 100 N=1,NL
      READ(1,6)X,PX
      WRITE (3,10) PX
      DSP=PX-P1
      DSOE=DSP*OEPL
      OEP=DSOE+OER
      GAMMA=(F0/OEP)*10000.
      OESQ=OEP**2
      IVOESQ=1.0/OESQ
      KEFF=((GAMMA-SGAMMA)/SGAMMA)*100.
      WRITE(3,9)GAMMA,KEFF
      WRITE(2,9)GAMMA,KEFF
      WRITE(2,8)X,OEP,IVOESQ
  100 WRITE(3,8)X,OEP,IVOESQ
      GO TO 300
  200 STOP
    1 FORMAT(20A4)
    2 FORMAT(3F10.4,1I2)
    3 FORMAT (2F10.4)
    4 FORMAT(1H1,20A4)
    6 FORMAT(    2F10.4)
    7 FORMAT(7H FREQ.=,E16.8,16H MHZ   FREQ.SQ.=,E16.8,6H MHZSQ)
    8 FORMAT(5H LINE,E16.8,5H   H=,E16.8,12H OE   H(-2)=,E16.8)
    9 FORMAT(7H GAMMA=,E16.8, 8H   KEFF=,E16.8,8H PERCENT)
   10 FORMAT(15HOLINE POSITION=,E16.8)
   12 FORMAT (11H FREQ.(-2)=,E16.8)
   13 FORMAT (13H HZ PER LINE=,E16.8,13H OE PER LINE=,E16.8)
      END
```

```
ERMN2 14.0198804 MHZ LINE -1 LN2 TEMP
FREQ.=  0.14019880E 02 MHZ    FREQ.SQ.=  0.19655704E 03 MHZSQ
FREQ.(-2)=  0.50875805E-02
HZ PER LINE=  0.11273318E-02 OE PER LINE=  0.10161629E 01

LINE POSITION=  0.80000000E 02
GAMMA=  0.10416161E 02    KEFF= -0.79847050E 00 PERCENT
LINE -0.10000000E 01    H=  0.13459738E 05 OE    H(-2)=  0.55198406E-08

LINE POSITION=  0.97000000E 02
GAMMA=  0.10402805E 02    KEFF= -0.92566347E 00 PERCENT
LINE -0.10999994E 01    H=  0.13477016E 05 OE    H(-2)=  0.55056972E-08

LINE POSITION=  0.11270000E 03
GAMMA=  0.10390507E 02    KEFF= -0.10427923E 01 PERCENT
LINE -0.12999992E 01    H=  0.13492969E 05 OE    H(-2)=  0.54926872E-08
```